Cold Regions Science and Technology, 11 (1985) 171–180
Elsevier Science Publishers B.V., Amsterdam – Printed in The Netherlands

DEFLECTION OF A FLOATING SEA ICE SHEET INDUCED BY A MOVING LOAD

Takatoshi Takizawa
Institute of Low Temperature Science, Hokkaido University, Sapporo 060 (Japan)

(Received May 9, 1984; accepted in revised form February 8, 1985)

ABSTRACT

A large number of time–deflection curves was obtained from a field experiment carried out on the sea ice sheet at Lake Saroma, Hokkaido, Japan, using a Skidoo snowmobile as a moving load with the test speed changed from 0 to 14.2 m/s. The thickness of the ice sheet was 0.17–0.18 m, the ice temperature was −2.5 to −4°C at the surface, and the water depth was 6.8 m beneath the ice sheet. The experimental results indicated the existence of a critical speed u_c and its value was estimated to be 5.8 m/s. At speed above it two ice waves were generated, one ahead of and the other behind the vehicle. A variation of wavelength with vehicle speed was expressed by a modified dispersion relation for the flexural ice wave in a floating ice sheet. The ice deflection pattern was classified into five stages. At u_c the depression around the vehicle was maximal in depth and minimal in width. The center of the depression began to lag behind the vehicle even at fairly low speeds below u_c.

INTRODUCTION

Floating ice sheets constitute an integral part of the human activities in cold regions, serving as ice crossings, airstrips and other transportation links. Obviously there is a need to establish a reliable safety criterion, which can only be accomplished by systematic studies of the response of the ice sheet to the load of a moving vehicle.

When the vehicle speed and the ice thickness have specific values, it is possible that an ice deflection under a moving vehicle is amplified markedly and simultaneously an ice wave begins to develop. This possibility, in which the specific vehicle speed is defined as the critical speed u_c, has been suggested and treated theoretically by Wilson (1958) and Nevel (1970), while its phenomena have been observed in field experiments (Wilson, 1958; Eyre and Hesterman, 1976; Eyre, 1977; Takizawa, 1978; Beltaos, 1979).

Wilson proposed a theory for predicting a generation of two different ice waves, one ahead of the load (leading wave) and the other behind it (trailing wave). On the basis of the experimental results, however, Eyre and Hesterman (1976) and Eyre (1977) concluded that the moving load generated only one orderly wave in front of it. Further, Beltaos (1979) observed the leading wave alone. Meanwhile, Takizawa (1978) found the generation of two waves, though the trailing wave disappeared at speeds not much greater than u_c. The ice wave is one of the substantial reactions of the floating ice sheet to the moving load, but the question whether or not the moving load generates two waves remains unsolved.

Thus, an extensive field experiment was conducted to clarify the characteristics of ice deflection patterns, e.g., number of waves, ice depression profile and vehicle's position. This paper will describe the experimental results and discuss some noticeable features of the ice response to the moving load.

OUTLINE OF THE EXPERIMENTAL SITE

The experiment was carried out from February 4–10, 1981, at Lake Saroma (44°10′ N, 143°50′ E) in Hokkaido, Japan. The lake is a large elliptical lagoon with a northwest–southeast length of about 26 km and a northeast–southwest width of about

0165-232X/85/$03.30

12 km. The basin is saucer-shaped, with a maximum water depth of 19.6 m.

The lake began to freeze at the end of January. The formed sea ice (7.7‰ in salinity) was very flat at its surface, on which a test track of 400 m in length was prepared parallel to the shoreline at a distance of about 1 km from the shore. The mean ice thickness, measured daily at three randomly selected points along the track, varied from 0.17 to 0.18 m during the experimental period. The mean water depth beneath the track was 6.8 m. The depth of snow cover ranged from 0.02 to 0.08 m during the experimental period.

Five L-tube glass thermometers were placed at depths of 0, 0.05, 0.1, 0.15, and 0.3 m from the ice surface, the upper four for the ice temperatures and the lowest for the water temperature. Another glass thermometer was used to measure air temperature. They gave the following temperatures in the day-time during the experimental period: the air temperature was −2 to −11°C, except on the afternoon of February 6 when it read −18.6°C; the ice temperatures were −2.5 to −4°C at the surface, −2.3 to −3.3°C at a depth of 0.05 m, −2.4 to −3.3°C at a depth of 0.1 m and −2.0 to −2.4°C at a depth of 0.15 m; the water temperature was constant, reading −1.8°C.

INSTRUMENTATION AND EXPERIMENTAL PROCEDURE

A Skidoo (2.43 m in length, 0.79 m in width, 235 kg in weight including a driver) was used as a moving load; in addition, another Skidoo (2.46 m in length, 0.935 m in width, 240 kg in weight including a driver) was used on 8th of February.

The ice deflection was measured with three deflectometers. They were potentiometric displacement transducers anchored to the lake bed by thin cables and installed each at an interval of 2 m midway between both ends of the track. They were aligned either parallel (D_1, D_2 and D_3 in Fig. 1) or normal (D_1', D_2 and D_3') to the direction of the track. The former set-up was called "along-track arrangement", and the latter "off-track arrangement".

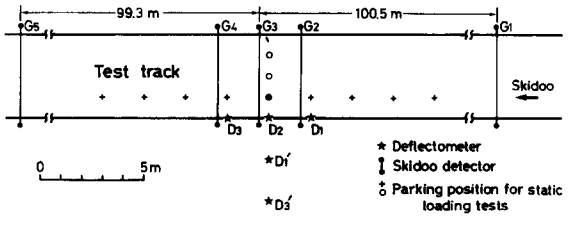

Fig. 1. Plan of experimental site at Lake Saroma.

To determine the location of the Skidoo, vehicle detectors were set at five points along the track as shown in Fig. 1 (G_1–G_5). The detector was a thin copper wire stretched over across the track. When a running Skidoo broke the wire, the microswitch connected to the wire generated a pulse signal. Three detectors (G_2, G_3, G_4) were located close to the deflectometers in such a manner that the detector worked the moment the center of the Skidoo passed the deflectometer.

The distance between the deflectometer and the center line of the Skidoo's trace was mostly 1 m for the "along-track arrangement", although some test runs were made at distances of 2 and 3 m. For the "off-track arrangement" test runs were carried out at distances between the center of Skidoo's trace and the nearest deflectometer D_2 of 1, 2 and 3 m.

The number of the test runs totaled 141, and the test speed ranged from 0 to 14.2 m/s. On each dynamic test run the Skidoo was quickly accelerated to the required speed before reaching the first Skidoo detector. The speed at which the Skidoo was driven through the track was maintained as constant as possible thereafter. The mean speed was calculated for each test run at the interval of 199.8 m between G_1 and G_5, and this speed was adopted as the test speed.

Static loading tests were included in dynamic test sequences. In case of the "along-track arrangement", the nine parking positions along the track were marked at an interval of 2 m, as shown in Fig. 1. The Skidoo moved slowly and stopped at each parking position for about half a minute successively, from the second to the eighth position on 5th of February and from the first to the ninth on 6th. In case of the "off-track arrangement", the Skidoo was parked at distances of 1, 2 and 3 m from the nearest deflectometer D_2 perpendicular to the direction of the track (see Fig. 1). These two arrangements gave a longitudinal and a transversal profile of ice deflection in the static loading tests.

EXPERIMENTAL RESULTS AND DISCUSSION

1. Static loading tests

In case of the "along-track arrangement", when the Skidoo was parked at the j-th position, the deflection of the i-th deflectometer $\delta_i(j)$ can be approximately regarded as the deflection at a distance of $2[(i+3)-j]$ m from the load, where i=1–3 and j=1–9. The obtained deflections, rearranged in accordance with the distance from the load, yielded the longitudinal profile, as shown in Fig. 2a. Meanwhile, tests for the "off-track arrangement" with the similar procedure yielded the transversal profile, as shown in Fig. 2b.

In the longitudinal profile, the positive and negative signs of the abscissa indicate that the distance is forward and backward with respect to the Skidoo, respectively. It is noticeable that the obtained profile lacked symmetry, i.e., the backward slope was steeper than the forward slope and the backward rim was considerably elevated. This asymmetry is believed to result from such a load distribution of the Skidoo that the load was concentrated on the rear. On the other hand, the transversal profile can be regarded as symmetrical, since the load distribution was symmetrical transversally.

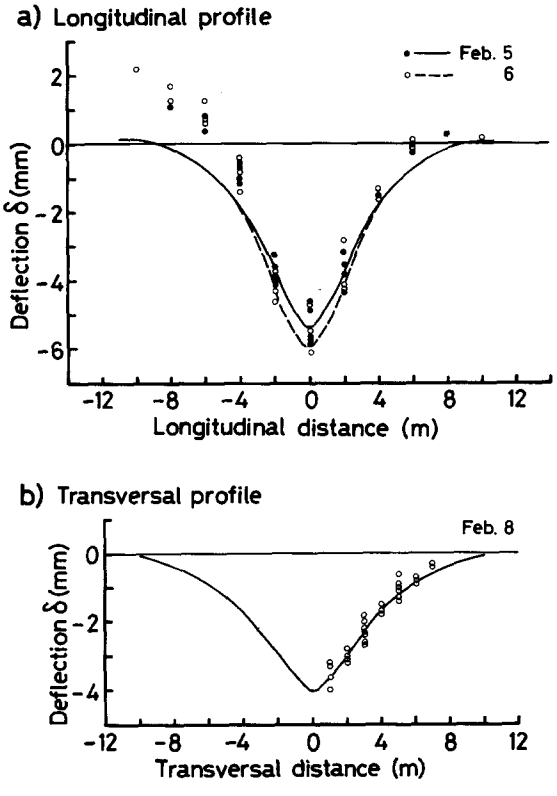

Fig. 2. Deflection profiles with static loading.

Assuming that an ice plate is homogeneous, isotropic and elastic, and rests on an elastic foundation of the Winkler type, Hertz (1884) showed for the first time a theoretical curve for the deflection profile with a static load. Later, the same result was given by the South Manchurian Railway Company (1941), Wyman (1950) and Kubo (1958a,b). For a concentrated load, Wyman predicted the deflection δ at the radial distance r from the load by the following equation

$$\delta(r) = \frac{P}{2\pi\rho L^2} \, Kei\,(r/L), \tag{1}$$

where P is the mass of the load, ρ the water density and "*Kei*" Kelvin's Bessel function of order zero. The symbol L is the characteristic length of the ice and is defined by

$$L = \left[\frac{Eh^3}{12\rho g(1-\sigma^2)}\right]^{1/4}, \tag{2}$$

where E and σ are the elastic modulus and Poisson's ratio for the ice, respectively, h the ice thickness and g the acceleration due to gravity.

Substituting the test data into eqn. (1), we obtain simultaneous equations in which only L is unknown. Assuming that L did not vary significantly during a daily test sequence, the best-fit L in the least-squares sense was calculated for all daily data with g = 9.8 m/s^2 and ρ = 1026 kg/m^3. Since the profile data given in Fig. 2 were not symmetrical for the longitudinal profile, the calculation was made using only the half-side data (forward of the Skidoo). Resultant values of L for each test data set are given in Table 1. The theoretical curves based on the values of L are plotted in Fig. 2. The curves are in good agreement with the data points, except for the backward data, which were not taken into account in derived L.

The obtained L values enabled us to calculate the corresponding values for E through eqn. (2) with an assumption of constant σ. Assuming σ=1/3, the values for E were obtained as shown in Table 1. It

TABLE 1

Results of static loading tests

Date	h (m)	P (kg)	$\bar{\delta}$* (mm)	L (m)	E ($\times 10^8$ N/m^2)	Remarks
Feb. 5	0.17	235	−5.4	2.3	6.1	longi-tudinal
Feb. 6	0.17	235	−5.4	2.2	5.1	longi-tudinal
Feb. 8	0.18	240	−3.5	2.7	9.8	trans-versal

*$\bar{\delta}$: Mean depression depth. Note that the deflection measurements were taken at a point 1 m from the center of the Skidoo's trace.

should be noted that they are of the same order of magnitude as those obtained by uni-axial compression tests (2.5×10^8 and 2.8×10^8 N/m^2; Takizawa, 1978).

2. Dynamic loading tests

The records of typical runs are shown in Fig. 3 for various vehicle speeds u. It was found that the deflection pattern, which changed with the speed, was classifiable into the following five typical stages, with the approximate speed range given in the brackets for each stage.

(1) Quasi-static stage [$0 < u < 3.5$ m/s ($0 < u/u_c < 0.6$)]. At low speeds, the deflection pattern was a dish-shaped depression surrounded by a slightly elevated rim. The overall pattern was similar to the static deflection curve shown in Fig. 2a. This fact suggests that the static profile is simply carried with the vehicle in this low speed range. The center of the depression, however, slightly lagged behind the vehicle.

(2) Early-transition stage [$3.5 \leqslant u < 5.0$ m/s ($0.6 \leqslant u/u_c < 0.86$)]. As the speed was increased, the depression became deeper and narrower. The rim around the depression rose progressively, and a small trough began to form ahead of the forward rim.

(3) Late-transition stage [$5.0 \leqslant u < 5.8$ m/s ($0.86 \leqslant u/u_c < 1$)]. With a further increase in speed, the depression continued to deepen and narrow. A wave-like pattern began to form at both the forward and the backward side of the depression, and simultaneously the lag of the depression center rapidly increased with the speed. These phenomena presaged a coming wave generation.

(4) Two-wave stage [$5.8 \leqslant u < 8.0$ m/s ($1 \leqslant u/u_c < 1.4$)]. At speeds just above the critical speed u_c, two different waves were generated, one with a relatively short wavelength in front of the vehicle and the other with a longer wavelength at the rear of the vehicle. As described later in Section 5, the critical speed u_c was estimated to be 5.8 m/s. The depression was maximal in depth and minimal in width at u_c. With an increase in speed, the depression reversed its previous trend and became progressively shallower and wider. The wavelength of the leading wave was shortened and that of the trailing wave was elongated with an increase in speed. The number of wave crests and the wave amplitude were reduced with increasing speed.

(5) Single-wave stage [8.0 m/s $\leqslant u$ ($1.4 \leqslant u/u_c$)]. At a speed not much greater than u_c, the trailing wave

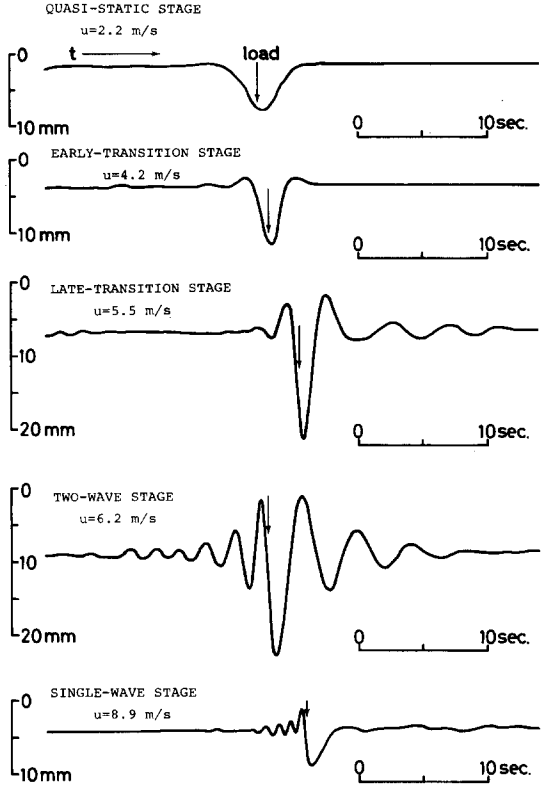

Fig. 3. Typical ice deflection records at various vehicle speeds, February 5, 1981.

disappeared, and the leading wave alone was observed.

The wave attenuated to zero amplitude over a distance of several wavelengths even at the beginning of the two-wave stage. The attenuation rate with respect to a distance increased with the vehicle speed. Hence this suggests that the attenuation of the ice wave depends not only on the distance but also on the vehicle speed.

It should be emphasized that the two-wave stage existed; in other words, the trailing wave was observed, though in a small region of speed. This wave has been predicted by Wilson (1958) and later observed by Takizawa (1978), while its existence has not been noticed in the other experiments conducted by Eyre (1977) and Beltaos (1979).

3. Propagation speed of the depression or ice wave

Eyre (1977) has mentioned that the speed of the generated ice wave was identical with the vehicle speed, because the vehicle maintained the same position relative to the ice deflection profile throughout each test run. In the present experiment it was possible to evaluate the propagation speed of the generated depression or ice wave directly through simultaneous recording of the ice deflection at three locations along the track.

An obtained relation between the propagation speed and the vehicle speed is shown in Fig. 4. Each value of the propagation speed was calculated by the average travelling time of distinct crests or the depression of the pattern for a distance between two deflectometers. It is indicated by the figure that the depression or wave was always propagated at the vehicle speed at any stage of the deflection pattern.

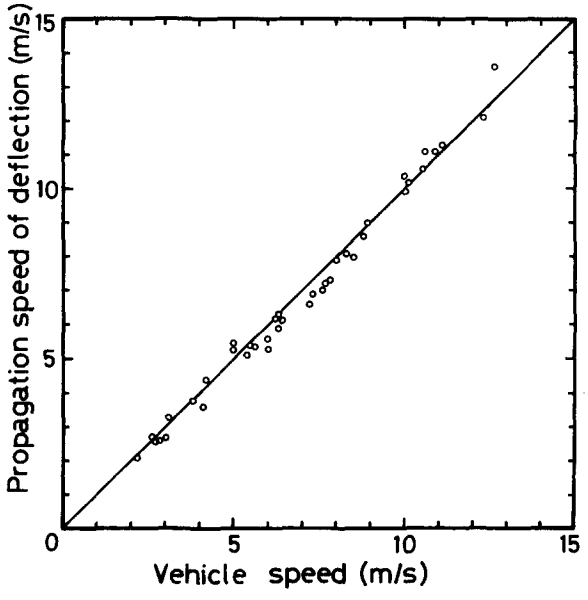

Fig. 4. Propagation speed of ice deflection pattern versus vehicle speed. The distance between the deflectometer and the vehicle's trace was 1 m.

4. Wavelength of the ice wave

The frequency of the ice wave f was determined directly from a time–deflection curve. The wave was found to propagate at the vehicle speed u; hence the wavelength λ was given by $\lambda=u/f$.

The variation of the wavelength with the vehicle

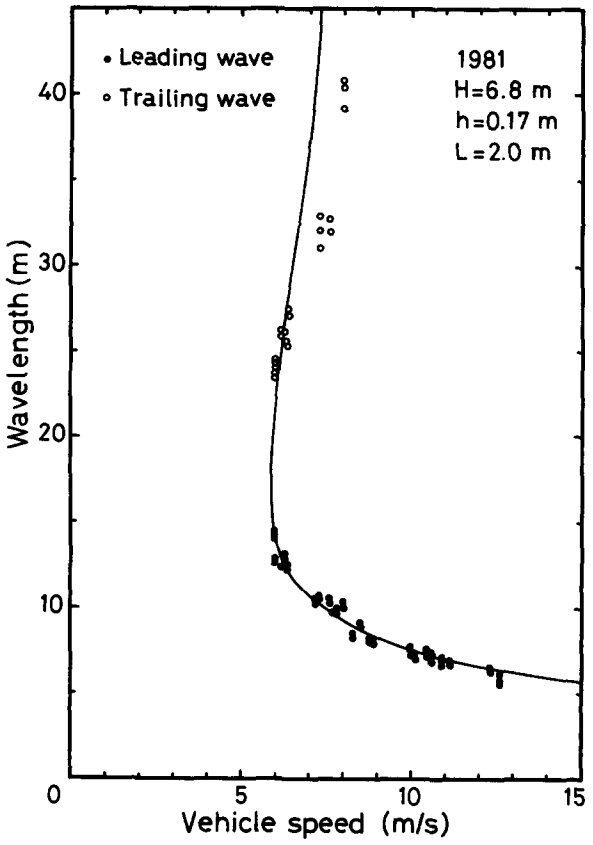

Fig. 5. Variation of wavelength with vehicle speed. The distance between the deflectometer and the vehicle's trace was 1 m.

speed is shown in Fig. 5. For the leading wave, λ decreased gradually with an increase in u. For the trailing wave, on the other hand, λ increased rapidly with u.

Wilson (1958) has derived the following dispersion relation between the phase velocity c and the wave number k for flexural waves in a floating ice sheet

$$c^2 = \frac{g}{k}(1+L^4k^4)\tanh kH, \tag{3}$$

where H is the water depth.

To incorporate the vehicle speed u in eqn. (3), Wilson assumed that a vehicle moving at speed u generated two waves having wavelengths consistent with the phase velocity $c=u$, and each of these waves then propagated at the group velocity, which was different from the vehicle speed. As mentioned in the previous section, however, the present experiment showed that the ice wave propagates at the same speed as the vehicle. Hence c in eqn. (3) can be replaced by u. Substituting $k=2\pi/\lambda$ in eqn. (3), we have the following theoretical relation between λ and u for the ice wave induced by the moving load

$$u^2 = \frac{g\lambda}{2\pi}\left[1+L^4\left(\frac{2\pi}{\lambda}\right)^4\right]\tanh\left(\frac{2\pi}{\lambda}H\right), \tag{4}$$

in which only L is unknown. The best-fit L in the least-squares sense was found to be 2.0 m for H= 6.8 m. The theoretical curve is plotted in Fig. 5. The curve agrees well with the data points. It is noted that L is slightly smaller than that obtained by the static loading tests (see Table 1). Thus the corresponding value for the elastic modulus E_{dynamic} calculated through eqn. (2) for h= 0.17 m is 3.5 X 10^8 N/m^2 and smaller than E_{static}. It is known that the E values obtained by dynamic methods are generally larger than those by static ones. Since the E values are strongly affected by the test conditions and scatter considerably (Weeks and Assur, 1967), this opposite result is due to the scattering and probably has no significant meaning.

5. Depth of the ice depression

The depression around the vehicle did not lose its identity at all speeds, though its configuration changed with the speed, as shown in Fig. 3. At the bottom of this depression, the ice deflection was always maximal. The variation of the depression depth with the vehicle speed is shown in Fig. 6. The depth increased at first with the vehicle speed and reached its maximum, which demonstrated the existence of the critical speed u_c. At speeds above it, the depression depth decreased quickly with an increase in speed, which became then comparable to the static values at $u \simeq 1.5u_c$ ($u \simeq 8.7$ m/s). With a further increase in speed, it continued to decrease gradually and its values were smaller than the static ones. The general trend of the variation is consistent with the previous experimental results (Wilson, 1958; Eyre, 1977; Takizawa, 1978; Beltaos, 1979) and a theoretical prediction by Nevel (1970).

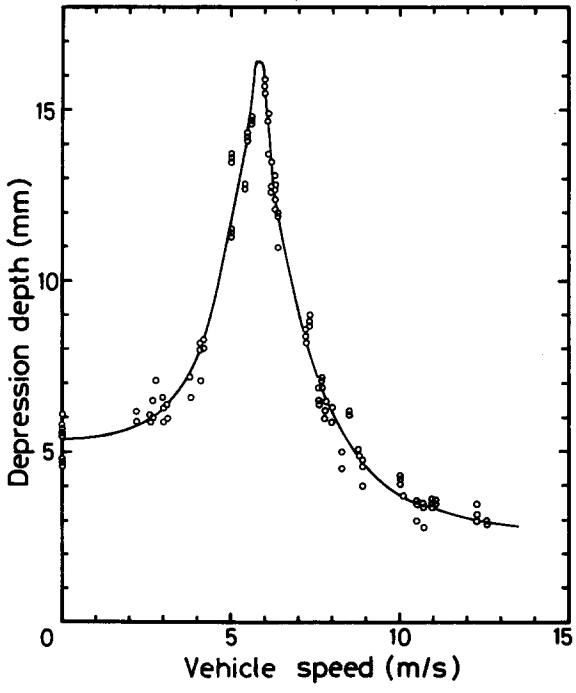

Fig. 6. Variation of depression depth, measured at a transversal distance of 1 m, with vehicle speed.

As described above, the depression depth had a maximum, showing a prominent peak. This peak was used to determine the value for u_c. The data points and trend curve suggested that u_c was in the range of 5.6–6.0 m/s. Consequently, it was reasonable to take their mean, 5.8 m/s, as u_c.

The measured depth at u_c was about three times

the depths under static loads, while according to the previous experiments it was approximately two (Eyre, 1977; Beltaos, 1979) to four times (Takizawa, 1978).

6. Depression width

The width of the depression curve was defined as the distance between the two points which intersected with the neutral line. The depression width also changed with the vehicle speed as shown in Fig. 7. The width decreased at first with an increase in speed and reached its minimum at u_c; above it the width rapidly increased and became greater than the width under static loads. This general trend is opposite to that of the depression depth shown in Fig. 6.

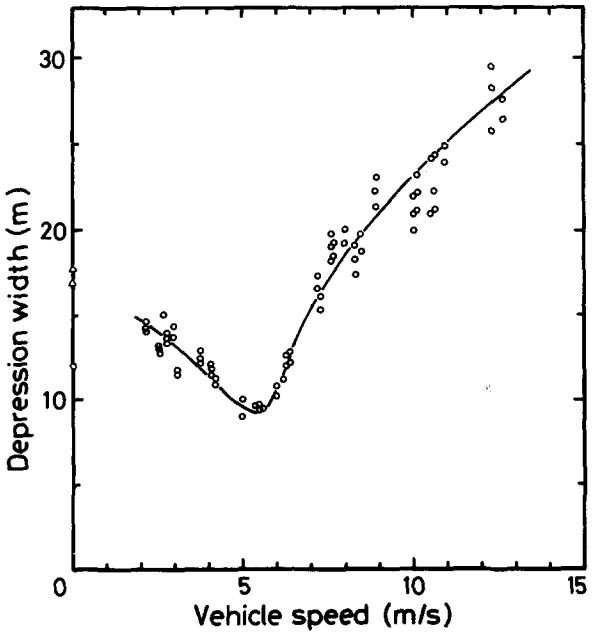

Fig. 7. Variation of depression width, measured at a transversal distance of 1 m, with vehicle speed. Δ – theoretical values.

Equation (1) predicts a depression width of $7.8L$, when the vehicle is at rest. For L= 2.2 and 2.3 m (Table 1), the width was estimated to be 17.2 and 17.9 m, respectively. The width obtained from Fig. 2a, however, is markedly smaller than the predicted values. As mentioned in the previous section, the depression depth was almost the same at u= 0 as at $u \simeq 1.5u_c$. If we assume that the width is also the same at u= 0 as at $u \simeq 1.5u_c$, similar to the variation of the depression depth, the theoretical values seem to be reasonable. A lack of data points at low speeds, however, does not permit a further argument on this large discrepancy.

7. Effect of in-plane forces on the critical speed

Recently Kerr (1979, 1983) showed that the critical speed u_c may be substantially affected by in-plane forces in an ice sheet: a compression force field reduces u_c, whereas a tension force field has the opposite effect. Ono (1976) estimated a constrained stress at 65 kPa by measuring constrained thermal strains in fast ice of 2.1 m thickness at Barrow, Alaska, U.S.A. Assuming that a laterally compressive stress due to wind blowing across a pack ice field is in the range of 0–70 kPa, Bates and Shapiro (1980) evaluated its effect on u_c. When the stress is 70 kPa for 1.5-m thick ice, u_c is reduced by only a few percents at most. Thus, for thick ice the magnitude of in-plane forces possible under the natural condition may have little effect on u_c.

Meanwhile, as for the thin ice used in the present experiment, Kerr's theory predicts that in-plane forces such as the magnitude of 70 kPa produce a noticeable effect.

Applied to the present experimental situation, Nevel's theory (1970), which does not include in-plane forces, predicts $u_c = 1.27\sqrt{gL}$. For L= 2.0 m, accordingly, u_c= 5.6 m/s. The experimental value of u_c is 5.8 m/s, so that the difference in u_c is fairly small. If this difference is significant and attributable to the effect of in-plane forces, it appears that the forces were very small, and hence u_c was little affected by them, though they were not measured in the experimental field.

8. Lag of the maximum deflection position behind the vehicle

As described earlier, the center of the depression lagged behind the vehicle. The lag time t_ℓ was transformed into the lag ℓ by $\ell = ut_\ell$. The relationship between ℓ, which was measured at a transversal distance of 1 m, and the vehicle speed is presented in Fig. 8. It is seen from the figure that ℓ increased rapidly with u for $u > 5$ m/s. This variation is identical

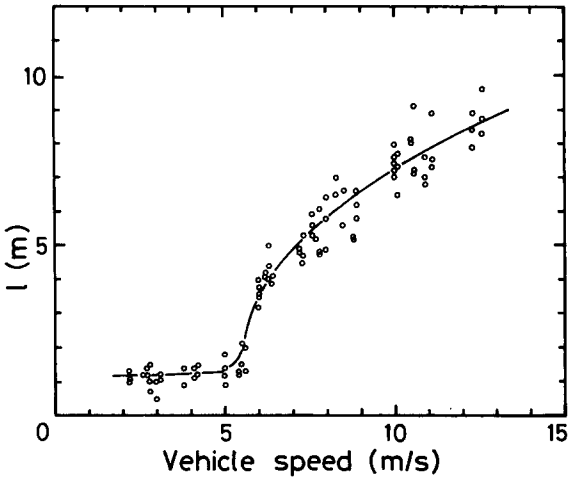

Fig. 8. Variation of the lag ℓ, measured at a distance of 1 m, with vehicle speed.

with that found by Takizawa (1978). Meanwhile, at low speeds such as below 5 m/s, the lag was almost constant, about 1 m. This differs from the previous experimental results, which demonstrated that the lag arises at a speed slightly below u_c; that is, at low speeds the lag does not occur (Eyre, 1977; Takizawa, 1978). Two factors may cause a virtual lag: an experimental error and the effect of transversal distance. An experimental error, which is due to the delay in wire breaking of the Skidoo detector, would make the lag decrease rather than increase. Thus it cannot cause the virtual lag. Figure 9 shows a dependence of the lag on the transversal distance d between the deflectometer and the center of the skidoo's trace at various vehicle speeds. Seven speed groups were differentiated by different symbols. The results showed that the lag decreased with decreasing d at every speed. Extrapolation of the data indicates that the lag is not zero at d= 0 m, even for a speed of 2.9 m/s. Accordingly, we can conclude that the lag occurs at a fairly low speed. This conclusion is supported by Kenney (1954), who presented an analytical solution for a moving load on a beam on an elastic foundation including the effect of viscous damping. Kenney's theory gives a non-dimensional plot of lag against vehicle speed U ($=u/u_c$) for various values of dimensionless damping factor B (Fig. 10). As is evident from the figure, even at speeds $U < 1$, the lag is not zero for $B \neq 0$. Furthermore, it can be seen that the curve for B= 0.1 is quite

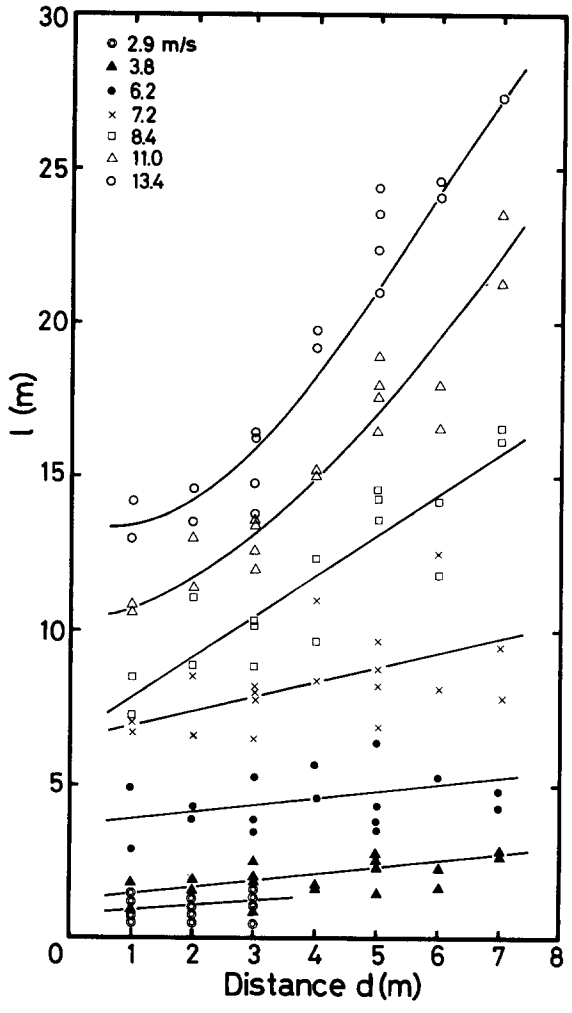

Fig. 9. Variation of the lag ℓ with the distance d at various vehicle speeds.

similar to the measured variation shown in Fig. 8; namely, the lag is fairly small for $U < 1$, and it increases sharply at $U \simeq 0.9$. Thus it follows from the facts mentioned above that the lag occurs for all speeds except 0 m/s, its magnitude is quite small for $u < u_c$, it increases markedly at a speed slightly below u_c, and the variation can be explained qualitatively in terms of small viscous damping. It should be noted that the lag is fairly small for $U < 1$, which most likely explains why Eyre (1977) and Takizawa (1978) did not notice it.

The lag time t_ℓ can be regarded as being comparable to the retardation time τ, which is one of the most important parameters in the viscoelastic

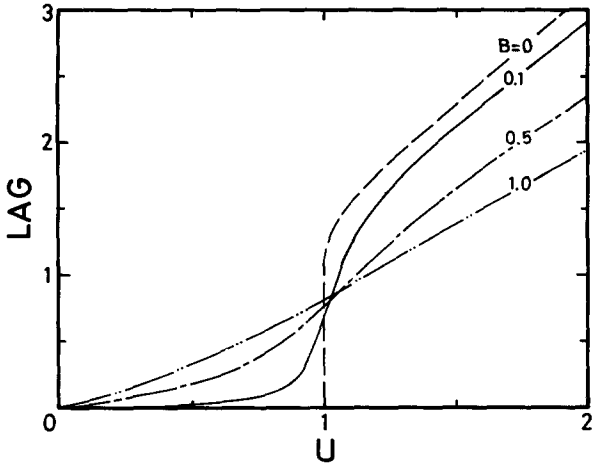

Fig. 10. Non-dimensional plot of lag against vehicle speed (after Kenney's theory, 1954). U is the non-dimensional vehicle speed defined by u/u_c, and B is the non-dimensional damping factor.

theory. Assuming that $\tau = t_\ell$, we can evaluate the viscosity coefficient for ice η, since τ is defined by $\tau = \eta/E$. Figure 11 is a plot of t_ℓ against u. A drastic jump of t_ℓ at a speed between 5.6 and 6.0 m/s suggests that the response nature of the ice sheet to the moving load changed substantially at the critical speed u_c = 5.8 m/s. The lag time is almost constant at speeds above 6 m/s, and the mean lag time is 0.69 s. The lag time is roughly in a range of 0.2–0.8 s. Choosing $E_{\text{dynamic}} = 3.5 \times 10^8$ N/m^2 for E, we have $\eta = 7 \times 10^7 - 2.8 \times 10^8$ N s/m^2. Taking the Maxwell unit as the viscoelastic model for sea ice, Tabata (1959) determined η by measuring the internal friction of rectangular ice bars. Its value was $3 \times 10^7 - 2 \times 10^8$ N s/m^2 at ice temperatures around -3°C. Thus the viscosity coefficients obtained in the present experiment agree well with those by Tabata.

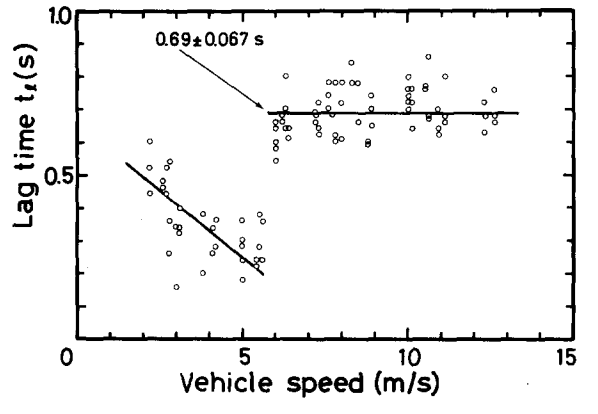

Fig. 11. Plot of lag time t_ℓ, measured at a distance of 1 m, against vehicle speed.

From Fig. 9 the transversal propagation of ice deflection can be figured out. The solid lines in Fig. 9 can be considered to show the plan view of the depression trough at the time when the vehicle moving along the ordinate downward reached the origin. It is obvious that the trough lines are oblique to the direction of motion, and the angle between them becomes sharp with increasing vehicle speed. This line also represents the position of the wave front for speeds above u_c= 5.8 m/s.

9. Relative position of the vehicle with respect to the depression

The ratio of the lag to the half width of the depression is shown in Fig. 12 against the vehicle speed. The ratio indicates the relative position of the vehicle with respect to the depression curve. Although the data points scatter markedly, it is found that the ratio increases rapidly at a speed near 5 m/s and then remains almost constant at speeds above 7 m/s. In other words, the vehicle stays slightly ahead of the depression bottom when its speed is below u_c, but it shifts its relative position very rapidly at speeds near u_c. At speeds above u_c the vehicle retains the relative position at approximately two-thirds up the forward slope of the depression.

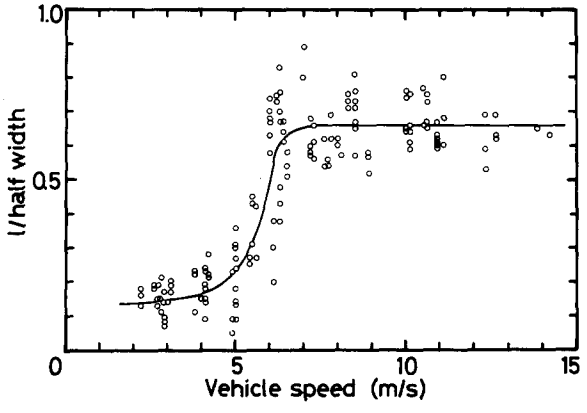

Fig. 12. Ratio of the lag ℓ to the half width of depression with vehicle speed. The distance between the deflectometer and the vehicle's trace was 1 m.

CONCLUDING REMARKS

The experimental results confirmed the existence of two ice waves against the contrary conclusion by Eyre (1977) that a moving load generates only one orderly wave in front of it. This discrepancy may be caused by a difference in instrumentation. The conventional bottom-anchored deflectometer used in the present experiment is so insensitive to high-frequency ice oscillations that it responds only to the primary mode of ice oscillation. Furthermore, it gives the direct reading of ice deflection. On the other hand, the deflectometer used by Eyre is a sensitive water pressure transducer. In his case the deflectometer response includes hydrodynamic pressure disturbances in addition to purely hydrostatic effects that reflect the ice deflection. As a result, the high-frequency fluctuations due to the pressure disturbances are expected to increase particularly in the vehicle's wake and obscure the primary response to the trailing wave.

ACKNOWLEDGMENTS

The author wishes to express his gratitude to the late Professor T. Tabata for the guidance and encouragement. He also wishes to express his deep thanks to M. Nakawo, N. Ono and Y. Suzuki for their valuable discussions and critical reading of the manuscript. Thanks are also extended to M. Oi and H. Fukushi for preparing the skidoo detectors and making the computer program used for the data processing. He acknowledges the assistance of M. Ishikawa and T. Motoi in the field tests.

REFERENCES

Bates, H.F. and Shapiro, L.H. (1980). Long-period gravity waves in ice-covered sea. J. Geophys. Res., 85 (C2): 1095–1100.

Beltaos, S. (1979). Fields studies on the response of floating ice sheets to moving loads. Proc. Workshop on the Bearing Capacity of Ice Covers, 16–17 October 1978, Winnipeg, National Research Council of Canada, Technical Memorandum No. 123: 1–13.

Eyre, D. and Hesterman, L. (1976). Report on an ice crossing at Riverhurst during the winter of 1974–1975. Saskatchewan Research Council, Report No. E76-9.

Eyre, D. (1977). The flexural motion of a floating ice sheet induced by moving vehicles. J. Glaciol., 19(81): 555–570.

Hertz, H. (1884). Ueber das Gleichgewicht schwimmender elastischer Platten. Wiedemann's Ann. Phys. Chem., 22: 449–455.

Kenney, J.T. (1954). Steady-state vibrations of beam on elastic foundation for moving load. J. Appl. Mech., 21: 359–364.

Kerr, A.D. (1979). The critical velocities of a floating ice plate subjected to in-plane forces and a moving load. U.S. Cold Regions Research and Engineering Laboratory, CRREL Report 79-19.

Kerr, A.D. (1983). The critical velocities of a load moving on a floating ice plate that is subjected to in-plane forces. Cold Reg. Sci. Tech., 6: 267–274.

Kubo, Y. (1958a). Loading capacity of ice plate (1). Seppyo, 20(3): 75–78 (in Japanese).

Kubo, Y. (1958b). Loading capacity of ice plate (2). Seppyo, 20(4): 97–104 (in Japanese).

Nevel, D.E. (1970). Moving loads on a floating ice sheet. U.S. Cold Regions Research and Engineering Laboratory, Research Report 261.

Ono, N. (1976). Arctic sea ice research. III. Measurements of state of thermal stress induced in surface layer of sea ice cover. Low Temp. Sci., Ser. A, 34: 221–226 (in Japanese).

South Manchurian Railway Company (1941). Kahyō tokuni hyōjōkidō ni kansuru kenkyū [Studies on river ice; with special reference to the construction of railroad on ice] (in Japanese).

Tabata, T. (1959). Studies on mechanical properties of sea ice. IV. Measurement of internal friction. Low Temp. Sci., Ser. A, 18: 131–148 (in Japanese).

Takizawa, T. (1978). Deflection of a floating ice sheet subjected to a moving load. II. Low Temp. Sci., Ser. A, 37: 69–78 (in Japanese).

Weeks, W.F. and Assur, A. (1967). The mechanical properties of sea ice. U.S. Cold Regions Research and Engineering Laboratory, CRREL Monograph II-C3.

Wilson, J.T. (1958). Moving loads on floating ice sheets. University of Michigan Research Institute (UMRI Project 2432).

Wyman, M. (1950). Deflections of an infinite plate. Can. J. Res., Ser. A, 28: 293–302.